Earth and Planetary Science Letters 520 (2019) 141–152

Contents lists available at ScienceDirect

Earth and Planetary Science Letters

www.elsevier.com/locate/epsl

New insights on the Orosirian carbon cycle, early Cyanobacteria, and the assembly of Laurentia from the Paleoproterozoic Belcher Group

Malcolm S.W. Hodgskiss [a,*], Olivia M.J. Dagnaud [b], Jamie L. Frost [b], Galen P. Halverson [b], Mark D. Schmitz [c], Nicholas L. Swanson-Hysell [d], Erik A. Sperling [a]

[a] Department of Geological Science, Stanford University, California, USA
[b] Department of Earth & Planetary Sciences, McGill University, Montréal, Québec, Canada
[c] Department of Geosciences, Boise State University, Boise, ID, USA
[d] Earth and Planetary Sciences Department, University of California, Berkeley, CA, USA

ARTICLE INFO

Article history:
Received 5 December 2018
Received in revised form 15 May 2019
Accepted 16 May 2019
Available online xxxx
Editor: D. Vance

Keywords:
Belcher Group
Paleoproterozoic
Orosirian
carbon cycle
Cyanobacteria
Nuna

ABSTRACT

The Orosirian Period (2050–1800 Ma) of the Paleoproterozoic Era represents an interval between the Great Oxidation Event and Lomagundi-Jatuli Excursion, and the apparent environmental stability of the late Paleoproterozoic to mid-Mesoproterozoic (1800–1300 Ma). Here, we present stratigraphic data, carbon isotope chemostratigraphy, element abundances, and U–Pb zircon depositional ages from the Belcher Group in subarctic Canada, providing an unparallelled global reference section for the Orosirian Period. U–Pb dates of 2018.5 ± 1.0 Ma and 2015.4 ± 1.8 Ma for two tuffs in the Kasegalik Formation (lowest Belcher Group) provide the first robust age constraints for Earth's earliest unambiguous cyanobacterial fossil, *Eoentophysalis belcherensis*. A tuffaceous shale ~4 km stratigraphically higher, at the contact of the Flaherty and Omarolluk formations (1854.2 ± 1.6 Ma), provides an age for foreland basin development associated with the collision of the Superior and Hearne cratons. Carbonate carbon isotope data show smooth fluctuations ranging from −2.3 to +3.6‰, reaching a maximum near ca. 1.88 Ga. This trend toward heavier carbon isotope values is interpreted as the result of global orogenesis during Nuna assembly that elevated nutrient supply and sedimentation rates, leading to an increase in the proportion of organic carbon burial relative to carbonate carbon burial.

1. Introduction

The Orosirian Period (2050–1800 Ma) of the middle Paleoproterozoic Era is bookended by two strongly contrasting times in Earth history. The preceding Great Oxidation Event (GOE; ca. 2.4–2.05 Ga) and associated Lomagundi-Jatuli Excursion (LJE) mark the appearance of free oxygen in the atmosphere and the largest, longest positive carbon isotope excursion in Earth history (Gumsley et al., 2017; Karhu and Holland, 1996). Subsequent to the Orosirian, the late Paleoproterozoic to mid-Mesoproterozoic (1800–1300 Ma) is an interval of inferred global environmental stability with a non-glacial climate, $\delta^{13}C$ confined to a relatively narrow range (generally −1 to 0‰), low gross primary productivity, and generally low atmospheric oxygen (Fiorella and Sheldon, 2017; Brasier and Lindsay, 1998; Crockford et al., 2018). The Orosirian Period is hypothesised to record a shift in the Earth system relative to the preceding GOE and LJE: a decline in atmospheric oxygen (originally suggested due to the reappearance of iron formations), a reduction in the size of the marine sulphate reservoir, and a return of carbonate carbon isotope values to near 0‰ (e.g., Canfield, 2005; Bekker and Holland, 2012; Scott et al., 2014). Nevertheless, few detailed carbonate geochemical studies have targeted this important transition in the Earth system, and existing geochemical data are low-resolution and lacking in robust stratigraphic and geochronological control. Consequently, even the most fundamental geochemical systems, such as the carbon cycle, remain poorly constrained during this 250 Myr interval.

The Belcher Group, of the eponymous archipelago in Nunavut, Canada, is a 7–10 km thick package of Orosirian-age carbonate and siliciclastic strata interrupted by two voluminous mafic volcanic formations (Figs. 1, 2; Jackson, 1960; Ricketts, 1979). Despite being well-preserved for a basin of this age (sub-greenschist metamorphic facies), containing a rich assemblage of microfossils (including the earliest unambiguous Cyanobacteria; Hofmann, 1976), an exquisitely exposed stromatolite reef complex, and an instance of the final major pulse of Paleoproterozoic iron formation (IF) deposition, the Belcher Group has received little study

* Corresponding author.
E-mail address: mswh@stanford.edu (M.S.W. Hodgskiss).

https://doi.org/10.1016/j.epsl.2019.05.023
0012-821X/

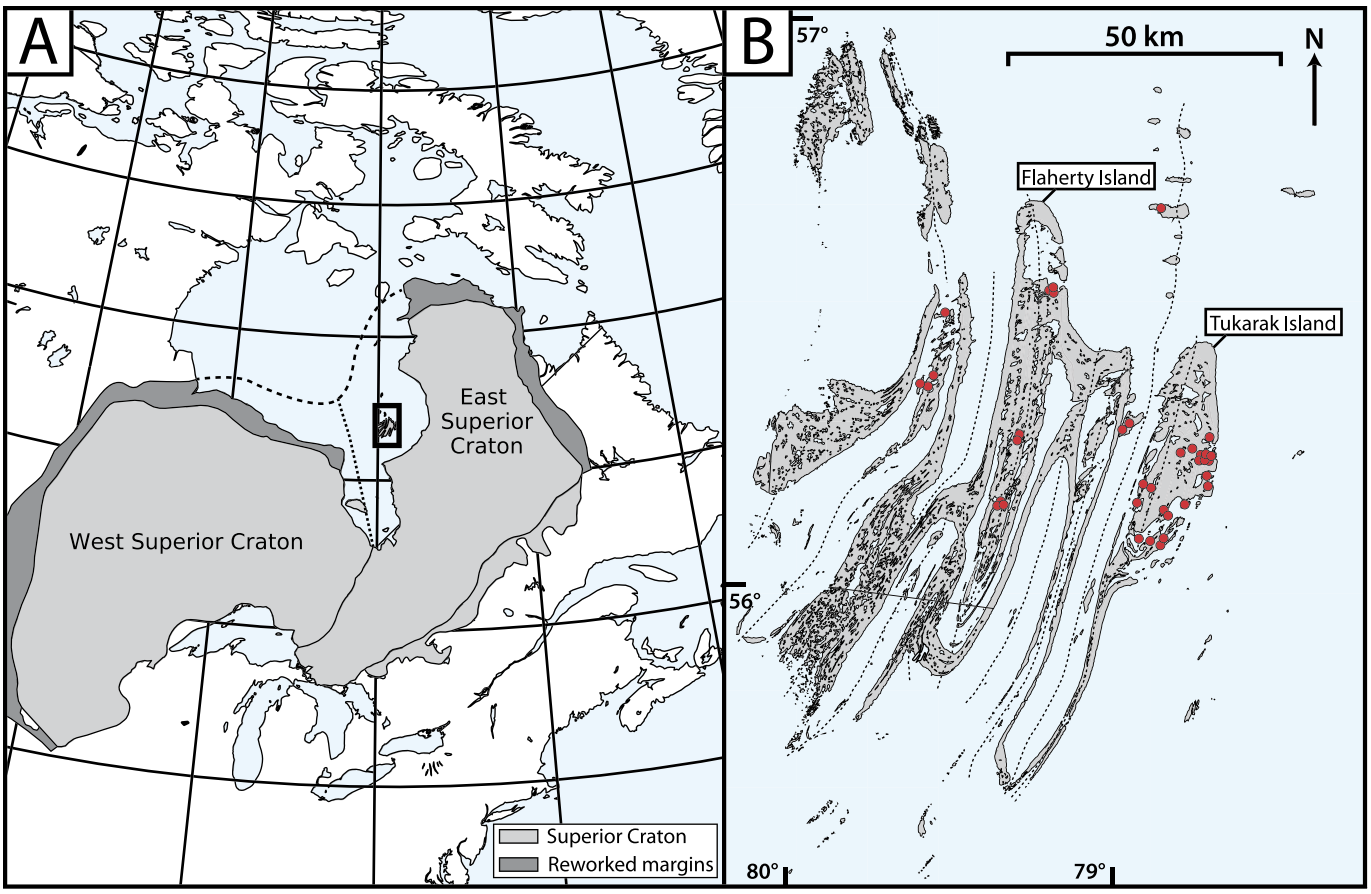

Fig. 1. A) Map of northeastern North America, with outlines of the exposed Superior Craton and reworked margins. Location of the Belcher Islands indicated by black box. Grey segment at SE margin of Superior Craton indicates where it is east of the Grenville Front. Polygons based on Whitmeyer and Karlstrom (2007). B) Map of the Belcher Islands, with locations of measured stratigraphic sections indicated by red circles. For a geological map refer to Fig. S1. (For interpretation of the colours in the figure(s), the reader is referred to the web version of this article.)

since the 1970s (Ricketts, 1979; reviewed by Jackson, 2013). Here, we present high-resolution $\delta^{13}C$ chemostratigraphy, element abundances, and zircon geochronology from the Belcher Group to test how the Orosirian carbon isotope record relates to the LJE and late Paleoproterozoic to mid-Mesoproterozoic records. Additionally, the new U–Pb dates constrain the age of the earliest unambiguous cyanobacterial microfossils, and combined with existing paleomagnetic data, provide new constraints on the assembly of Laurentia. Finally, stratigraphic data on the occurrence of evaporite minerals places an estimate on Orosirian marine sulphate concentrations.

2. Geological context

The Belcher Group overlies the northwestern margin of the Superior Craton. Structural deformation is most intense in the western part of the archipelago, where strata are slightly overturned or dipping near-vertically, and decreases markedly toward the eastern edge, where the strata are shallowly dipping. On the eastern shore of Hudson Bay, the nearly flat-lying Nastapoka Group (likely correlative to the Belcher Group; Baragar and Scoates, 1981), overlies Archean crystalline rocks of the Superior Craton. Thus, although the basement underlying the Belcher Group is not exposed on the archipelago, it is likely comprised of similar Superior Craton crystalline lithologies.

Based on available age constraints and similarities in stratigraphy and igneous geochemistry, the Belcher Group is part of the Circum-Superior Belt of Orosirian-aged basins in northeastern North America (Baragar and Scoates, 1981). However, previously published geochronology for the Belcher Group is sparse; a whole-rock Pb-Pb isochron of basalt from the Eskimo Formation yielded an age of 1960 ± 160 Ma (Arndt and Todt, 1994), and baddeleyite from two samples of Haig intrusions yielded indistinguishable U–Pb dates of 1870.3 ± 0.7 and 1870.1 ± 1 Ma (Hamilton et al., 2009). In the Richmond Gulf Group, which underlies the Nastapoka Group, diagenetic apatite cements have been dated as 2025 ± 25 Ma (Chandler and Parrish, 1989). These data suggest an age of ca. 2025 Ma for the Belcher Group, assuming it is correlative with the Richmond Gulf and Nastapoka groups, though this link has yet to be verified.

The Belcher Group is composed of subequal thicknesses of carbonates, siliciclastics, and mafic volcanic rocks (Fig. 2). The lowest 1.1 km of the exposed stratigraphy are comprised of carbonate rocks (Kasegalik Formation; Fig. 3A) deposited in sabkha to shallow subtidal settings. These strata contain the oldest known cyanobacterial fossil, *Eoentophysalis belcherensis* (Hofmann, 1976). They are followed by 0.2–1.0 km of primarily subaerially erupted basalt (Eskimo Formation) and 1.7–2.6 km of carbonate rocks again deposited primarily in a shallow marine setting (Fairweather, McLeary, Tukarak, Mavor, Costello, Laddie formations; Fig. 3B, C, D). The overlying series of mixed carbonate and siliciclastic rocks records continued deposition in shallow environments, including tidally-influenced siltstone, sandstone, and dolograinstone (350 m; Rowatt Formation) giving way to tidally-influenced sandstones with cross-cutting channels (120 m; Mukpollo Formation; Fig. 3E), then granular IF (130 m; Kipalu Formation; Fig. 3F). The Kipalu Formation is regarded as correlative to other ca. 1880 Ma IFs in

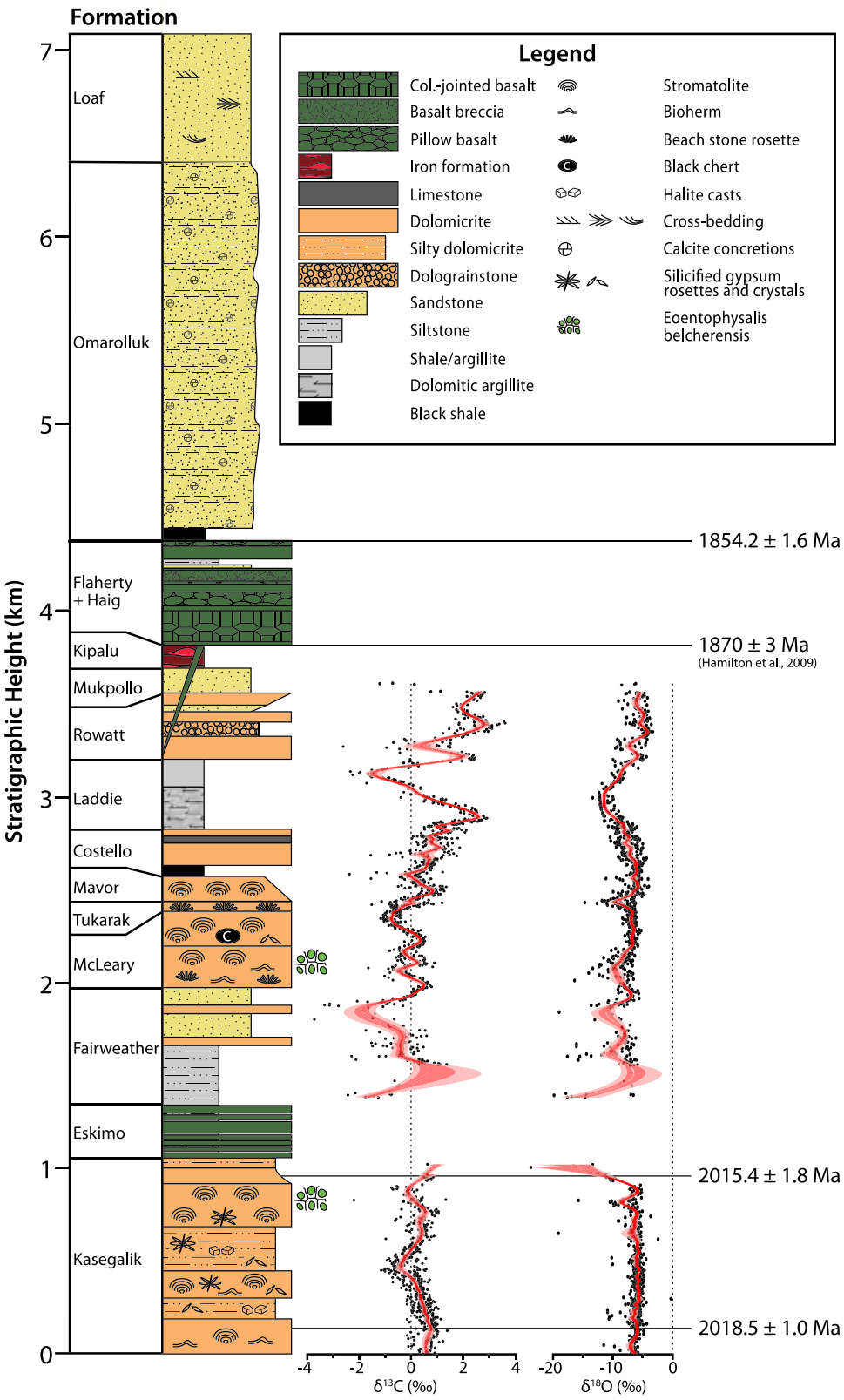

Fig. 2. Simplified stratigraphy of the Belcher Group and $\delta^{13}C$ and $\delta^{18}O$ data. Note that due to variations in lateral thickness, largely in volcanic units, the total thickness of the Belcher Group varies between 7 and 10 km. Light red and medium red shaded areas correspond to 2σ and 1σ uncertainty on the LOWESS regression (red line), respectively, from 20,000 bootstraps. $\delta^{13}C$ data exhibit variations of $\pm 1‰$ superposed on a trend from approximately 0 to 3‰. $\delta^{18}O$ data average approximately $-6‰$, with several lighter intervals. Note that the Laddie Formation records a strongly diagenetic signal, likely from the formation of authigenic carbonate. Spans used for fitting of LOWESS curves were determined using the R package fANCOVA, yielding spans of 0.1312 and 0.0991 for $\delta^{13}C$ and $\delta^{18}O$ in the lower segment, and 0.0507 and 0.0526 in the upper segment, respectively.

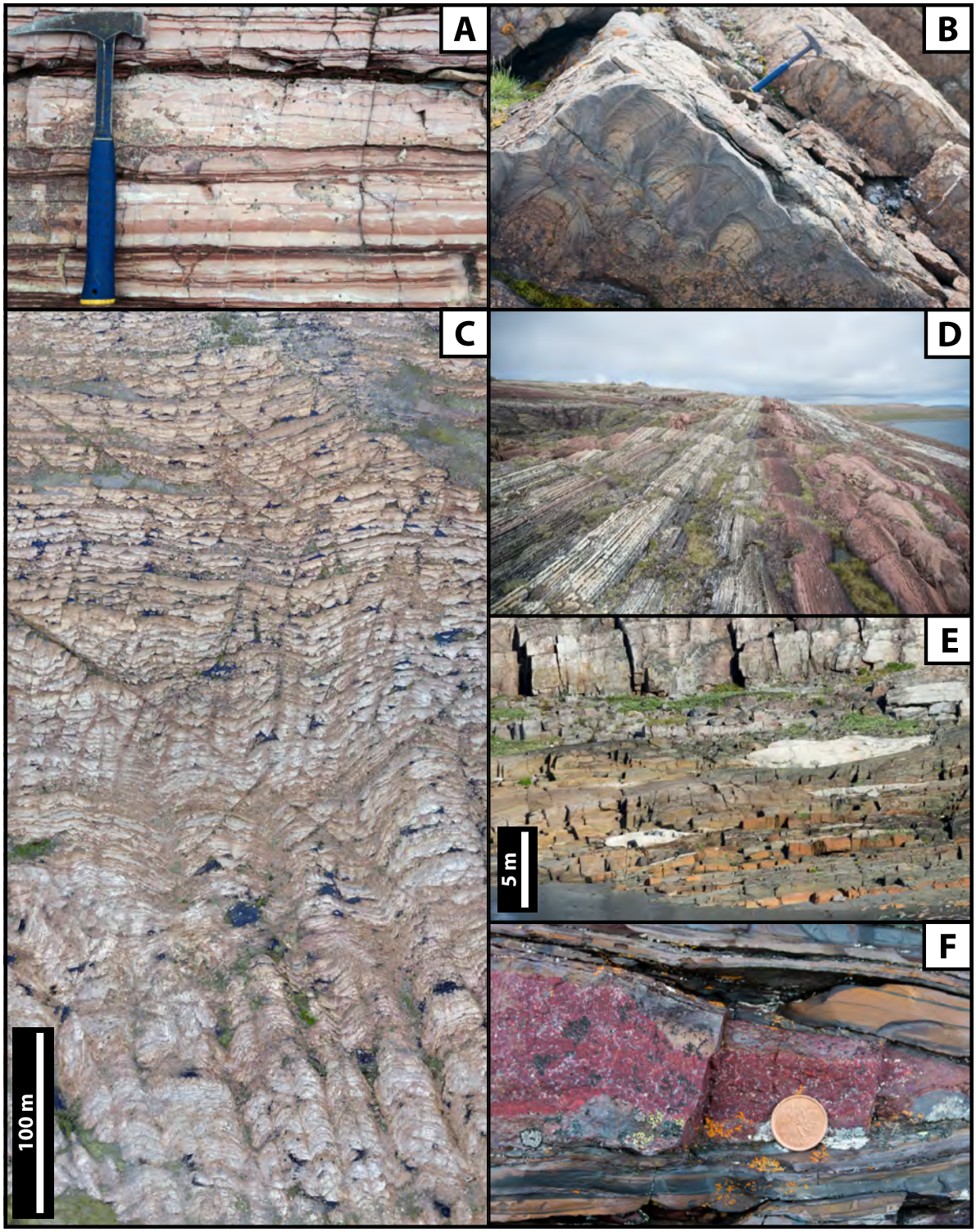

Fig. 3. Lithologies and sedimentary structures of the Belcher Group. A) Typical beige to pink dolomicrite of the Kasegalik Formation, with very thin interbeds of maroon argillaceous/silty dolomicrite. Thin horizons of intraformational rip-up clasts (centre) are common throughout the Kasegalik Formation, as is soft-sediment deformation (below centre). B) Stromatolites at the McLeary-Tukarak Formation contact. The orange bed of columnar stromatolites (beside hammer) marks the base of the Tukarak Formation and occurs throughout the eastern Belcher Islands. C) Drone photomosaic of the Mavor Formation stromatolite reef complex on eastern Tukarak Island. Approximately 200 m thick, the reef consists of broad stromatolite domes with several meters of relief that broaden and coalesce upward. D) Variably coloured carbonate sedimentary rocks of the Costello Formation. The weathering-resistant beds are composed of dolomicrite, whereas the thin, recessive interlayers are limestone. E) In the Mukpollo Formation, isolated channels of mature quartz sandstone several meters thick and up to 10 m wide cut into siltstones. F) Granular iron of the Kipalu Formation occurs as lenses and nodular horizons within variably iron-rich shales and siltstones.

the Circum-Superior Belt, such as the Gunflint IF in the Lake Superior region and Sokoman IF in the Labrador Trough (Rasmussen et al., 2012). It is followed by 0.2–2 km of largely submarine basalt (Flaherty Formation) and associated Haig feeder dykes and sills that intrude the Flaherty Formation and all underlying stratigraphy, but none of the younger stratigraphy. The overlying Omarolluk Formation consists of at least 3.3 km of turbidites, followed by at least 0.65 km of intertidal to fluvial siliciclastics (Loaf Formation), interpreted as prograding foreland basin flysch and molasse, respectively (Ricketts, 1979).

3. Methods

3.1. Carbon and oxygen isotopes

Carbon ($\delta^{13}C$) and oxygen ($\delta^{18}O$) isotope ratios of carbonates were measured in the Stable Isotope Laboratory at McGill University, using a NuCarb sample preparation device coupled to a Nu Instruments Perspective isotope ratio mass spectrometer (IRMS). Isotopic data are reported in standard delta notation relative to VPDB, and reproducibility of $\delta^{13}C$ and $\delta^{18}O$ measurements are 0.1‰ and 0.2‰ (2σ), respectively, based on repeat analyses of standards during the analytical runs (for detailed methods refer to Supplementary Materials).

3.2. Major/minor/trace elements

Analyses of major, minor, and trace element abundances were carried out at Institut Universitaire Européen de la Mer, Université de Bretagne Occidentale. A gentle leaching process (5% acetic acid) was used to prevent the dissolution of non-carbonate minerals (e.g., clays; for detailed methods refer to Supplementary Materials). Measurements were conducted using an Elemental Scientific 2DX autosampler coupled to a Thermo Scientific ELEMENT XR high-resolution inductively coupled plasma mass spectrometer (HR-ICPMS). Repeat analyses of the CAL-S standard reference material yielded 1-σ uncertainties of $\leq$9% for Ca, Mg, Mn, and Sr, and 12% for Fe.

3.3. Geochronology

All geochronological analyses were carried out in the Isotope Geology Laboratory at Boise State University. Zircons were mounted in epoxy, ground to their centres for cathodoluminescence (CL) imaging, and then analysed with a tandem in situ – isotope dilution workflow. Details of the laser ablation inductively coupled plasma mass spectrometry (LA-ICPMS) and chemical abrasion isotope dilution thermal ionisation mass spectrometry (CA-IDTIMS) methods are described in Macdonald et al. (2018). LA-ICPMS trace element geochemistry and U–Pb ages were used to rapidly screen out xenocrystic cores and reworked crystals from pyroclastic event beds, and identify young grain populations from detrital volcanic sandstones. Select grains were extracted and analysed by CA-IDTIMS for high precision ages, using the BSU-1B mixed isotope tracer calibrated to the EARTHTIME gravimetric solutions (Condon et al., 2015; McLean et al., 2015). Final ages are interpreted from CA-IDTIMS $^{206}Pb/^{238}U$ dates, in order to circumvent the sensitivity of $^{207}Pb/^{206}Pb$ dates to systematic errors in the ^{235}U decay constant and the natural $^{235}U/^{238}U$ ratio (Schoene et al., 2006; Mattinson, 2010; Hiess et al., 2012), which manifests as a slight positive discordance of closed system zircon when using the values recommended by Steiger and Jäger (1977). CA-IDTIMS dates are reported with weighted mean uncertainties given as X/Y/Z, where X is the 2σ analytical uncertainty, Y is the combined analytical and tracer uncertainty, and Z is the combined analytical, tracer, and decay constant uncertainty.

4. Results

4.1. Carbon and oxygen isotopes

A total of 1630 samples were collected from 36 measured stratigraphic sections throughout the Belcher Group for $\delta^{13}C$ and $\delta^{18}O$ analyses (Fig. 2). In the lower Belcher Group (Kasegalik – Mavor formations), $\delta^{13}C$ values are generally near 0‰ with variation of ±1‰. Starting at the upper Mavor Formation, $\delta^{13}C$ values increase to approximately +3‰ at the Costello – Laddie contact, before declining to −2.3‰. $\delta^{13}C$ values recover to +2 to +3.6‰ in the Rowatt Formation, the youngest unit with a significant proportion of carbonate strata. Overall, the $\delta^{13}C$ data in the Belcher Group exhibit a trend of increasing values from 0 to +3‰, with superposed fluctuations on the order of ±1‰, with the exception of a shift of −4‰ in the Laddie Formation. $\delta^{18}O$ values are generally near −6‰, with five intervals of lower $\delta^{18}O$ values (Fig. 2). These $\delta^{13}C$ and $\delta^{18}O$ trends are reproducible across stratigraphic sections up to 50 km apart (in present-day coordinates without palinspastic restoration).

4.2. Major/minor/trace elements

To better understand the impact of dolomitisation and diagenesis on the sample set, a total of 152 carbonate samples were analysed for their elemental compositions. The stratigraphic resolution of these data is approximately 30 m through the carbonate portions of the stratigraphy (Figs. S8–S15). A deliberately gentle leaching process was used, resulting in incomplete carbonate dissolution; typical Ca concentrations range from 10 to 12.5 wt%, although there are elevated intervals in the Kasegalik and Costello formations, and low intervals in the Fairweather, Laddie, and Rowatt formations. Mg concentrations range from 6 to 10 wt%, with low intervals in the Kasegalik, Fairweather, Laddie, and Rowatt formations. Normalisation to the predicted weight percent for pure dolomite (or calcite for samples with low Mg/Ca ratios) shows that samples typically contained ~60 wt% leachable carbonate. Fe concentrations generally range from 1,000 to 5,000 ppm, with peaks in the Fairweather, Laddie, and Rowatt formations reaching up to 33,500 ppm. Mn concentrations are typically near 200 ppm, but with elevated values peaking at 5,000 ppm in the Fairweather, Laddie, and Rowatt formations. Sr generally ranges from 6 to 60 ppm, with local peaks in the Kasegalik, Fairweather, Laddie, and Rowatt formations (up to 180 ppm). Mg/Ca ratios are consistently between 0.9 and 1.1 (mol/mol), except for a small number of samples in the uppermost Kasegalik Formation and the Laddie Formation. Mn/Sr ratios (mol/mol) generally range from 5 to 10, but reach highs of 120, 270, and 75 in the Fairweather, Laddie, and Rowatt formations, respectively. Fe/(Ca+Mg+Fe) ratios (mol/mol) are generally near 0.005, but reach highs of 0.16 in the Fairweather and Costello formations, 0.29 in the Laddie Formation, and 0.20 in the Rowatt Formation.

4.3. Geochronology

Three volcanic tuffs as well as the youngest detrital grains from two sandstones within the Belcher Group were analysed to provide depositional age constraints. Field photographs, photomicrographs, CL images, XRF thin section element maps, and detailed descriptions are reported in the Supplementary Materials. From sandstones in the middle Kasegalik Formation, 498 LA-ICPMS spot analyses yielded dominantly Archean provenance, with a minor number of Paleoproterozoic grains. CA-IDTIMS analysis of this youngest population ($n = 5$) of detrital zircons yielded a maximum depositional age of 2120.6 ± 1.2/1.5/2.5 Ma; these grains could be

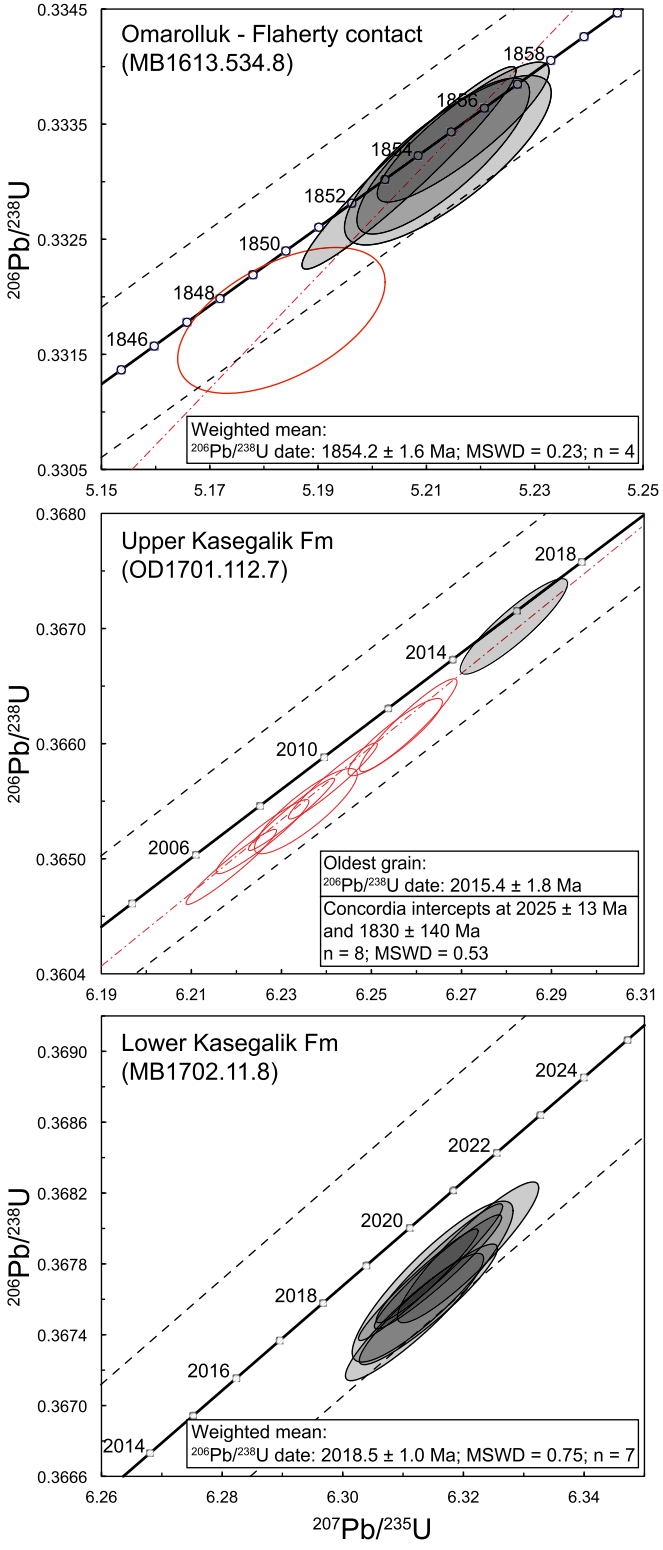

Fig. 4. U–Pb concordia diagrams for three volcanic tuffs from the Belcher Group. All measurements are on single zircon grains or fragments thereof, and ellipses shown in red are not included in the final age calculation.

sourced from volcanics related to the regional Marathon N and Biscotasing dyke swarms (Ernst and Bleeker, 2010). A volcanic lapilli tuff (sample MB1702.11.8, Figs. 4, 5A) approximately 150 m above the lowest exposure of the Kasegalik Formation yielded an eruptive age of 2018.5 ± 0.5/1.0/2.1 Ma (n = 7). A volcanic crystal tuff (sample OD1701.112.7, Fig. 5B) approximately 100 m below

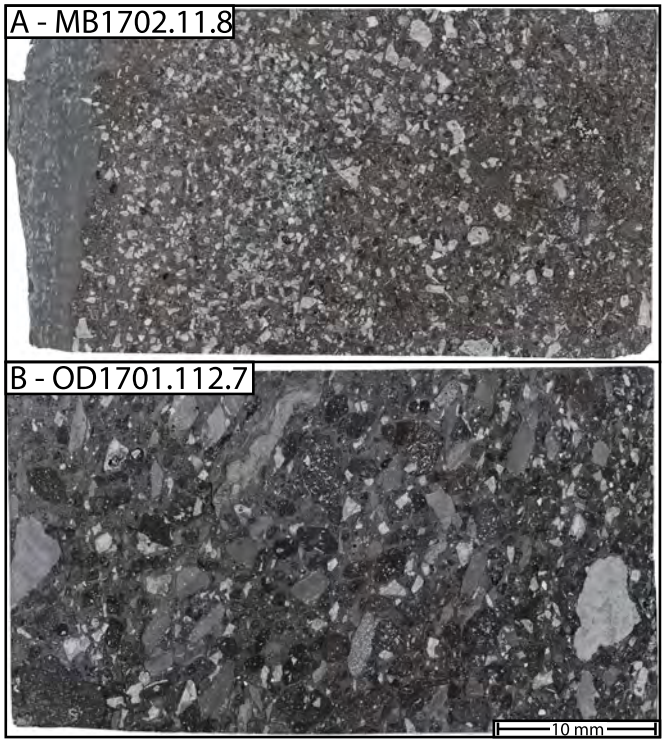

Fig. 5. A) Transmitted light photomicrograph mosaic from MB1702.11.8. This sample is composed largely of volcanic plagioclase and pumice lapilli. Contact with dolomicrite at left edge is the upper boundary of the tuff, and the sample therefore exhibits normal grading from porphyritic pumice lapilli to coarse ash dominated by free feldspar crystals (right to left). B) Transmitted light photomicrograph mosaic from OD1701.112.7. This sample contains abundant altered pumice lapilli (dark clasts exhibiting filled vesicles, spherulitic textures, and feldspar phenocrysts), lithic fragments of dolomicrite from the enclosing Kasegalik Formation, and large fragmented volcanic plagioclase crystals. Spherulitic textures are visible under cross-polarised light. Both images are to the same scale. For larger photomicrographs and corresponding XRF element maps, please refer to Supplementary Materials.

the Kasegalik–Eskimo Formation contact produced a slightly discordant array of single zircon analyses, from which we interpret a depositional age of 2015.4 ± 1.6/1.8/2.6 Ma from the oldest, most concordant analysis. Persistent discordance despite chemical abrasion likely records partial grain recrystallisation during fluid flow associated with ca. 1.83 Ga Trans-Hudson orogenesis (Weller and St-Onge, 2017). Finally, a sparse population of silt-sized zircons from a tuffaceous shale 5 m above the Flaherty–Omarolluk contact (sample MB1613.534.8) yielded an eruptive age of 1854.2 ± 1.4/1.6/2.4 Ma (Fig. 4; Table 1).

5. Discussion

5.1. Supercontinental assembly, basin evolution, and paleogeography

Deposition of the Belcher Group spanned from the opening of the Manikewan Ocean on the (present-day) northwestern margin of the Superior Craton to its subsequent closure associated with the Trans-Hudson orogeny (Pehrsson et al., 2016). The new U–Pb zircon dates from the Belcher Group provide robust constraints on this Wilson Cycle. Rapid (~3 Myr) accumulation of the ~1 km of shallow-water sediments of the Kasegalik Formation likely resulted from fault-driven generation of accommodation space associated with rifting ca. 2018 Ma. This rapid sediment accumulation rate is consistent with the interpretation that the Eskimo Formation volcanics are rift-related (e.g., Ricketts, 1979), but also indicates that rifting was ongoing prior to volcanism in the Belcher Group. A paleomagnetic pole from the Eskimo Formation (Schmidt, 1980)

Table 1
Stratigraphic position, coordinates (using the WGS 84 datum), and geochronological results of tuffs analysed.

Sample	Stratigraphic position	Latitude	Longitude	Age (Ma)	X (2)	Y (2)	Z (2)	MSWD	Grains used in age calculation (N)
MB1613.534.8	Lowest Omarolluk Fm, ~5 m above Omarolluk–Flaherty contact	N 56.284362°	W 78.958924°	1854.2	1.4	1.6	2.4	0.23	4
OD1701.112.7	Upper Kasegalik Fm, ~100 m below Kasegalik–Eskimo contact	N 56.154579°	W 79.336959°	2015.4	1.6	1.8	2.6	N/A	1
MB1702.11.8	Lower Kasegalik Fm, ~150 m above lowest exposure of Kasegalik Fm	N 56.350971°	W 79.558372°	2018.5	0.5	1.0	2.1	0.75	7

shares a common mean with that of the 1998 ± 2 Ma Minto dyke swarm (Fig. S27; Buchan et al., 1998). This paleomagnetic similarity and the new dates from the Kasegalik Formation support an association of the Eskimo Formation with the ca. 2000 Ma Minto large igneous province (Hamilton et al., 2016), although this mafic magmatism may have resulted from crustal thinning (that resulted in the generation of accommodation space in the Kasegalik Formation) rather than a plume. The similarity in pole positions between the Eskimo Fm, the Minto dykes and the Nastapoka basalts on the mainland east of the Belcher Islands support an interpretation that the Belcher Group is (para)autochthonous with the East Superior Craton (see Supplementary Materials). The paleomagnetic pole for the Eskimo Formation, along with poles for the younger Haig intrusions and Flaherty Formation volcanics (Schmidt, 1980), provide paleolatitude constraints on the Belcher Group. The basin was at 28° latitude (± 12°; 2σ) ca. 2000 Ma, and a similar latitude of 26° (±7°) ca. 1870 Ma, following the period of passive-margin sedimentation. Despite these similar paleolatitudes at ca. 2000 and 1870 Ma, the paleomagnetic poles indicate a large change in the orientation of the east Superior Craton, implying significant differential (i.e. rotational) plate tectonic motion over the time interval between the pole constraints.

The thick turbidite succession of the Omarolluk Formation, above the Flaherty Formation, is interpreted to have been deposited in a foreland basin associated with the Trans-Hudson orogen between the Superior and Hearne cratons and associated terranes (Hoffman, 1987). The date of 1854.2 ± 1.6 Ma from the base of the Omarolluk Formation indicates that collisional orogenesis was ongoing at that time and that the terminal collision that incorporated the Belcher Group into the fold-thrust belt had likely not yet occurred. This collision was central in the assembly of Laurentia and the amalgamation of Nuna, with assembly hypothesised to be complete ca. 1.6 Ga (Pehrsson et al., 2016).

A depositional age of 1854.2 ± 1.6 Ma for the base of the Omarolluk Formation is also significant because it only slightly precedes the age of the Sudbury impact event (1850 ± 1 Ma), approximately 1,100 km away (Krogh et al., 1984). These ages suggest that ejecta from the Sudbury impact event may occur stratigraphically above the dated tuff in the Omarolluk Formation. Although an ejecta layer was not observed in the field, the lower portion of the Omarolluk Formation is relatively poorly exposed, and outcrops in few locations. A detailed examination of the outcrops available, or a drill core through this interval, would help to test if ejecta from the Sudbury impact event are preserved in the Belcher Group.

5.2. $\delta^{13}C$: primary or secondary?

Before considering any potential implications of the stable isotope data presented here, it is important to consider how post-depositional processes may have impacted the original isotopic compositions, either by diagenetic alteration of the samples or formation of authigenic carbonate. Using element (Mg/Ca, Mn/Sr, and Fe/(Ca+Mg+Fe)) and isotope ratios ($\delta^{13}C$, $\delta^{18}O$), the importance of diagenesis and/or authigenic minerals was evaluated for each formation with a significant carbonate component. Meteoric alteration and burial diagenesis (increasing Mn/Sr) will generally result in decreasing $\delta^{18}O$ values, whereas dolomitisation (increasing Mg/Ca ratios) can increase $\delta^{18}O$ (Brand and Veizer, 1980; Land, 1980). The formation of authigenic siderite ($FeCO_3$) will incorporate remineralised organic matter, lowering the bulk-rock $\delta^{13}C$ value, while increasing the Fe/(Ca+Mg+Fe) ratio (e.g., Heimann et al., 2010). Finally, we use leached carbonate wt% to evaluate the proportion of the rock composed of calcite and dolomite, where lower values indicate a less carbonate-buffered sample that is more susceptible to diagenesis or the formation of authigenic minerals.

$\delta^{18}O$ values often exhibit a positive relationship with Mg/Ca, consistent with the relationship documented by Land (1980) related to dolomitisation (Figs. S8F–S15F). Combined with their very light compositions relative to modern carbonates, the $\delta^{18}O$ values reported here likely reflect secondary processes rather than a primary seawater signal. A generally positive relationship between $\delta^{18}O$ and carbonate wt% suggests that the most carbonate-rich samples are more likely to retain a higher $\delta^{18}O$ isotopic value.

Concerning $\delta^{13}C$, the Kasegalik, McLeary, and Costello formations exhibit no relationship between $\delta^{13}C$ and element systematics, suggesting that diagenesis, including dolomitisation, likely did not fundamentally alter depositional $\delta^{13}C$ signatures. The Fairweather, Mavor, Laddie, and Rowatt formations do exhibit relationships between $\delta^{13}C$ and element systematics, and therefore require further consideration. The Fairweather Formation exhibits positive relationships between $\delta^{13}C$ and carbonate wt% ($R^2 = 0.60$; Fig. S9C) and Fe/(Ca+Mg+Fe) ($R^2 = 0.90$; Fig. S9D). However, this relationship is largely controlled by the four samples with lightest $\delta^{13}C$, which exhibit the lowest Mg+Ca values and high Fe/(Ca+Mg+Fe) values. We therefore interpret these anomalously light $\delta^{13}C$ values as resulting from the formation of authigenic carbonate in strata with only a small primary carbonate component, shifting the bulk carbonate $\delta^{13}C$ toward lighter values. This process can similarly explain the occurrence of moderately depleted $\delta^{13}C$ values in the Mavor Formation, which coincide with enriched Fe/(Ca+Mg+Fe) ratios ($R^2 = 0.66$; Fig. S12D). The Laddie Formation exhibits a large shift in $\delta^{13}C$ from near +3.0 to −2.3‰, but this shift can be explained using the same mechanisms: there is a positive relationship between $\delta^{13}C$ and carbonate wt% ($R^2 = 0.56$; Fig. S12C), and a strong negative relationship between $\delta^{13}C$ and Fe/(Ca+Mg+Fe) ($R^2 = 0.90$; Fig. S12D). We therefore interpret the "excursion" toward negative $\delta^{13}C$ values in the Laddie Formation as resulting from the formation of authigenic carbonate (including siderite) in otherwise carbonate-poor sediments, shifting the bulk $\delta^{13}C$ toward negative values. Finally, the Rowatt Formation similarly exhibits relationships between $\delta^{13}C$ and carbonate wt% ($R^2 = 0.47$; Fig. S15C) and Fe/(Ca+Mg+Fe) ($R^2 = 0.75$; Fig. S15D). However, these relationships only occur in the carbonate-poor portions of the lower Rowatt Fm, rather than the formation as a whole.

To conclude, we consider the $\delta^{13}C$ of carbonate rocks from the Belcher Group to reflect primary seawater values, with the exception of the anomalously light $\delta^{13}C$ values (relative to the adjacent

stratigraphy) and rapid shifts toward negative $\delta^{13}C$ that occur most dramatically in the Laddie Formation, but also in the intermittently carbonate-poor strata of the Fairweather, Costello, and Rowatt formations. These isotopically-depleted $\delta^{13}C$ values can be explained through a process where the formation of a small amount of authigenic carbonate, including siderite, in relatively carbonate-poor rocks shifted bulk $\delta^{13}C$ toward more negative values. These data are therefore excluded from subsequent consideration in the discussion of the Orosirian carbon cycle.

5.3. The Orosirian carbon cycle

Carbon isotope ratios of marine carbonates reached extremely high values (5–15‰) during the LJE (ca. 2300–2060 Ma; Karhu and Holland, 1996; Gumsley et al., 2017), then were dominantly −1 to 0‰ for much of the late Paleoproterozoic through mid-Mesoproterozoic (1800–1300 Ma; e.g., Brasier and Lindsay, 1998). However, the transition between these two starkly different intervals – essentially represented by the Orosirian Period – is sparsely documented (e.g., Karhu and Holland, 1996; Bekker et al., 2016). The new data presented here fill a critical gap in the Proterozoic carbon isotope record. These data show a return of $\delta^{13}C$ values to near 0‰ following the end-LJE, by 2018.5 Ma (Fig. 2). If the isotopically-enriched $\delta^{13}C$ values identified by Bekker et al. (2016) in the ca. 2030 Ma Wooly Dolomite of Western Australia are representative of globally-elevated $\delta^{13}C$, the combined geochronological and $\delta^{13}C$ data presented here suggest that marine DIC returned to ∼0‰ by 2018.5 Ma. By the time of Mavor–Rowatt formation deposition, there is a clear trend toward higher $\delta^{13}C$ values and variability, reaching a maximum of +3.6‰. While $\delta^{13}C$ values up to approximately +2.5‰ have been previously reported in the late Paleoproterozoic to mid-Mesoproterozoic (e.g., Guo et al., 2013), the relatively high $\delta^{13}C$ values reported here are not unique only because of their enrichment, but also in their long-term trend toward increased $\delta^{13}C$ values, which contrasts with the 1830–1430 Ma interval for which high-resolution, time-calibrated $\delta^{13}C$ data exist (Fig. 6).

It is difficult to evaluate the global nature of the Belcher Group $\delta^{13}C$ trend given the absence of comparable long-duration, high-resolution, time-calibrated carbon isotope data sets through the Orosirian Period. However, the general $\delta^{13}C$ trend observed in the Belcher Group is consistent with the sparse global and regional records. Elsewhere in the Circum-Superior Belt, the Mistassini Basin contains carbonate rocks deposited shortly after the LJE, recording values near 0‰ (Bekker et al., 2007). In the ca. 1.88–1.865 Ga Pethei Group, Northwest Territories, Canada, $\delta^{13}C$ varies between −1 and 2‰ (Hotinski et al., 2004). The Belcher Group data also lie within the range of values found in large compilations of Proterozoic carbon isotope data (e.g., Shields and Veizer, 2002), although much of these data are generally from studies with poor age constraints and comparatively small sample sets. From an oceanographic perspective, the Belcher Group was likely sampling the global ocean; if the 1.88 Ga IFs are the result of increased iron supply to the oceans by intense volcanism (e.g., Hoffman, 1987; Rasmussen et al., 2012), the occurrence of granular IF in the Kipalu Formation demonstrates that the Belcher Group was at least intermittently connected to a body of water that circled almost the entirety of the Superior Craton. It therefore seems probable that these $\delta^{13}C$ data from the Belcher Group are representative at a global scale.

In order to place these new $\delta^{13}C$ data in the global record, it is important to consider the completeness of the stratigraphic record in the Belcher Group. Although the sedimentary record is generally highly incomplete, no large erosional unconformities or surfaces of non-deposition have been identified in the Belcher Group (Jackson, 1960; Ricketts, 1979; Jackson, 2013). Making the approximation of a constant sediment accumulation rate over the duration of the Belcher Group, an age of ca. 1940–1880 Ma can be inferred for the Mavor through Rowatt formations.

The $\delta^{13}C$ chemostratigraphic data presented here indicate that the defining characteristic of the Orosirian $\delta^{13}C$ record is the long-term increase toward values as enriched as 3.6‰. Interpreting the Proterozoic carbon cycle using the sedimentary record remains challenging, as the $\delta^{13}C$ recorded by sedimentary carbonate rocks is subject to many variables, with numerous non-unique solutions. Changes in the isotopic difference between organic and carbonate carbon, for example, could result in a systematic shift in $\delta^{13}C$. Additional variables, such as changes in weathering of organic and carbonate carbon, the isotopic composition of volcanic carbon, and the methane reservoir complicate matters further (Miyazaki et al., 2018). However, it is impossible to control for such factors from one site alone. Below we explore one possible cause for this positive carbon isotope shift, while remaining cognisant that carbon isotope records are increasingly recognized to represent a wider range of solution space than changes in organic carbon burial. Specifically, we look to the ancient tectonic record to explore this shift in $\delta^{13}C$, which may have been a consequence of the ongoing assembly of Nuna (Pehrsson et al., 2016) and a resulting increase in the proportion of organic carbon burial relative to carbonate carbon burial (f_{org}).

The assembly of the Nuna supercontinent involved a protracted interval of accretion and collisional orogenesis, and it is difficult to ascribe “peak Nuna orogenesis” to a single time (Pehrsson et al., 2016). Nonetheless, deposition of the Belcher Group coincided with a number of large orogenies associated with the amalgamation of Laurentia: the Thelon (ca. 1970–1920 Ma), initial phase of the Snowbird (ca. 1910–1865 Ma), Nagssugtoqidian (ca. 1880–1865 Ma), Wopmay (ca. 1880–1840 Ma), Penokean (ca. 1880–1840 Ma), Great Falls (1870–1720 Ma), Torngat (1870–1850 Ma), Trans-Hudson (1860–1820 Ma), and New Québec (1820–1770 Ma) orogenies all overlap in time with deposition of the Belcher Group (Fig. 6; Tirrul and Grotzinger, 1990; Berman et al., 2007; Kolb, 2014; Wardle et al., 2002; Hoffman et al., 2011; Skipton et al., 2016; Weller and St-Onge, 2017; Whitmeyer and Karlstrom, 2007, and references therein). These orogenies involved numerous cratons (Rae, Slave, Hearne, Wyoming, North Atlantic, Superior, Churchill) and terranes (Pembine-Wausau, Marshield, Nahanni, and others; Whitmeyer and Karlstrom, 2007) that collided to form Laurentia.

Beyond the well-constrained orogenic record of Laurentia, we look to the zircon record. The large compilation (∼150,000 zircons from all continents, including Greenland) of Barham et al. (2019) shows a distinct peak in zircons ca. 1850 Ma, more than any other time between 2050–1400 Ma. However, the exact meaning of the zircon record remains debated, specifically whether peaks represent enhanced crustal growth, recycling, or preservation. In the first scenario, the ca. 1850 Ma zircon peak would represent the generation of significant amounts of juvenile crust, whereas if crustal recycling is more significant (scenario two), the peak would represent increased subduction-related magmatism and crustal assimilation (Voice et al., 2011). Alternatively, it is possible that the ca. 1850 Ma zircon peak represents increased crustal preservation, which may be most favoured during the collision stage of supercontinent assembly (Voice et al., 2011). Finally, orogenic and post-orogenic plutons exhibit high zircon fertility, which would further increase the ca. 1850 Ma zircon peak (Moecher and Samson, 2006). Thus, although the underlying causes of peaks in the zircon population remain debated, they uniformly rely on enhanced tectonism/orogenesis as a fundamental mechanism. In this way, the zircon record reinforces a relationship between $\delta^{13}C$ in the Belcher Group and orogenesis, as the rise in zircon production is remarkably coincident with the rise in $\delta^{13}C$ observed in the Belcher Group

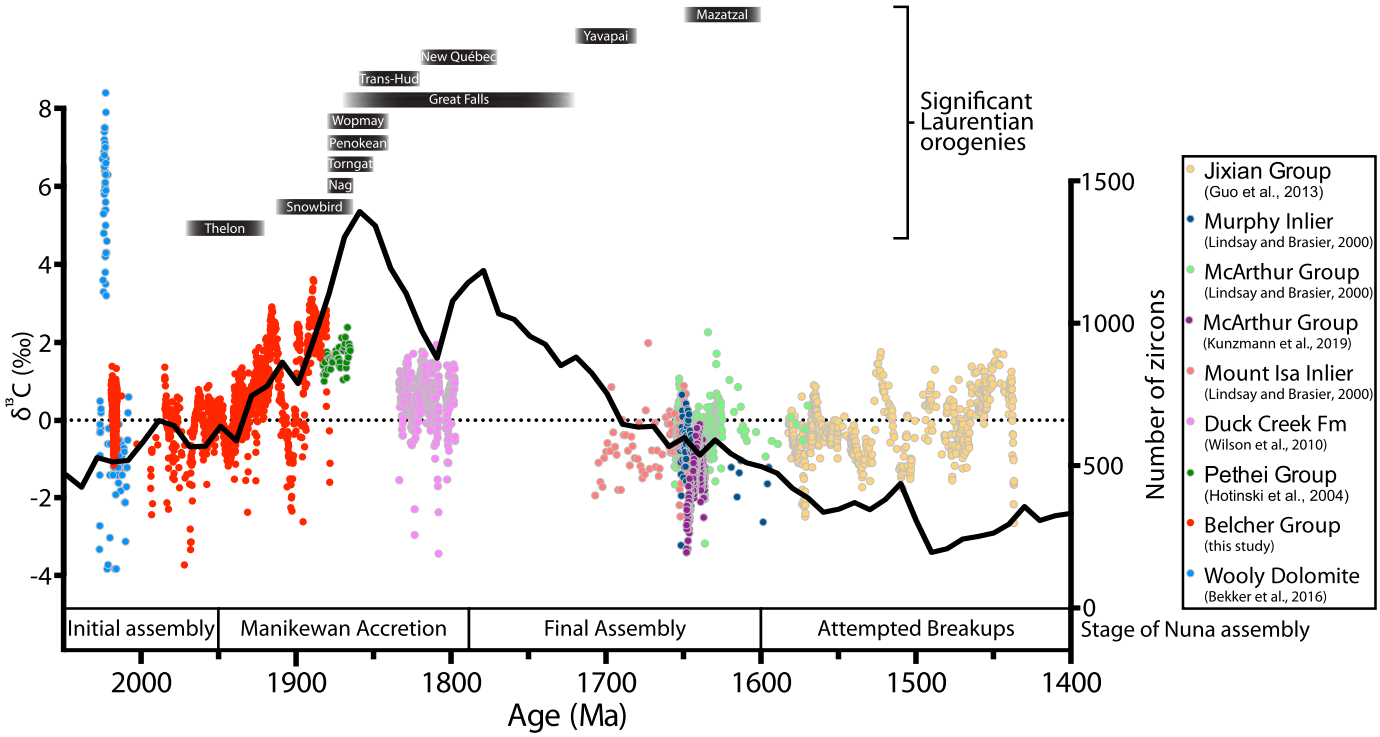

Fig. 6. Compilation of carbonate $\delta^{13}C$ data from basins around the world spanning approximately 2050–1400 Ma. Significant Laurentian orogenies indicated by black bars (note: Nag = Nagssugtoqidian; Trans-Hud = Trans-Hudson; Tirrul and Grotzinger, 1990; Berman et al., 2007; Kolb, 2014; Wardle et al., 2002; Hoffman et al., 2011; Whitmeyer and Karlstrom, 2007; Skipton et al., 2016; Weller and St-Onge, 2017). Black line indicates zircon population in 10-Myr bins using data from Barham et al. (2019). $\delta^{13}C$ values in the Belcher Group start near 0‰, and show an overall rise to approximately 3.6‰ in the Rowatt Formation, the highest formation with a significant proportion of carbonate rocks. Very shortly after the deposition of the Rowatt Formation is a hypothesised peak in accretionary orogenesis (Pehrsson et al., 2016), a potential driver for this shift in $\delta^{13}C$ values. Only studies with high-resolution $\delta^{13}C$ data and two or more robust depositional age constraints were used. Depositional rate is assumed to be constant between each pair of depositional ages. Whereas most data from this ca. 650 Myr interval show fluctuations around 0‰ with no apparent systematic variation, the $\delta^{13}C$ data presented here from the Belcher Group show a shift toward increased $\delta^{13}C$ values starting ca. 1940 Ma, coincident with a large increase in zircon population. $\delta^{13}C$ data are from Bekker et al. (2016), Hotinski et al. (2004), Wilson et al. (2010), Lindsay and Brasier (2002), Kunzmann et al. (2019), and Guo et al. (2013). Samples from the Belcher Group that are interpreted to have a diagenetic/authigenic component were not removed because similar screening techniques could not be applied to all data sets.

(Fig. 6). Indeed, the $\delta^{13}C$ peak in the Rowatt Formation was likely deposited only very shortly before 1.88 Ga, a time that Pehrsson et al. (2016) have hypothesised as a pulse of accretionary orogenesis during the assembly of Nuna. However, we note that the trend of increasing $\delta^{13}C$ may continue after deposition of the Rowatt Formation (in keeping with the orogenic and zircon record), although this is not recorded in the Belcher Group due to the cessation of carbonate sedimentary rock deposition. Thus, while the peak in Nuna orogenesis remains debated, deposition of the Belcher Group and an increase in $\delta^{13}C$ clearly overlapped with an interval of intense orogenesis in Laurentia and elsewhere.

There are several distinct mechanisms by which intense orogenesis could have increased f_{org}. The surface area of detrital sediments is an important factor in organic carbon burial (Hedges and Keil, 1995), and a large increase in sedimentary fluxes (with a correspondingly large increase in sediment surface area) to continental margins could have therefore increased f_{org}. France-Lanord and Derry (1997) noted that the Himalayan orogen – Bengal fan system alone comprises approximately 15% of the modern organic carbon burial flux. The Trans-Hudson orogen (recorded in the Omarolluk and Loaf formations in the Belcher Group), has been interpreted as analogous to the Himalayan orogen with regards to scale (~3,000 km long), tectonic evolution, and metamorphic grade (Weller and St-Onge, 2017), supporting the possibility that sufficiently large orogenic events were occurring during the Orosirian Period to have shifted f_{org}. Increased sedimentation rates on continental margins could also have increased f_{org} by increasing the efficiency of organic carbon burial (Canfield, 1994). An additional consideration is the role that orogenesis plays in nutrient supply to the oceans. Orogenesis would increase uplift rates, increasing physical weathering and ultimately the amount of material available for chemical weathering, enhancing the available nutrient supply (Waldbauer and Chamberlain, 2005).

5.4. The persistence of an Orosirian sulphate reservoir

Bedded sulphate minerals have been reported in a drill core from the ca. 2.1 Ga Tulomozero Formation (Blättler et al., 2018), and are followed by an interval with only sparse bedded sulphate evaporites, the most prominent of which occur in the ca. 1.05 Ga Angmaat Formation of the Bylot Supergroup in northern Canada (Kah et al., 2001; Gibson et al., 2017). This interval concludes with occurrences of thickly bedded sulphate minerals in strata in northwestern Canada and Australia closely associated with the Bitter Springs carbon isotope anomaly (ca. 811 Ma; e.g., Turner and Bekker, 2016). The sparse record of bedded sulphate minerals through this >1 Gyr interval, combined with sulphur isotope data, have led to the suggestion of a rapid decline in the size of the marine sulphate reservoir in the aftermath of the GOE (Scott et al., 2014). The evaporite minerals in the Belcher Group occur near the beginning of this interval and the hypothesised decline in the size of the marine sulphate reservoir. Halite casts, gypsum pseudomorphs, and microbarite are commonly preserved in the Kasegalik Formation (Fig. S24, S25), whereas the stratigraphically higher McLeary Formation contains only rare gypsum pseudomorphs, and no halite casts (Fig. S26; Bell and Jackson, 1974). The occurrence of only gypsum in the McLeary Formation indicates that waters reached gypsum saturation, but not halite saturation, and that gyp-

sum therefore precipitated prior to halite during deposition of the McLeary Formation. If the Orosirian ocean had modern calcium concentrations, these observations imply that marine sulphate concentrations were at least 2.5 mM (Schröder et al., 2008) ca. 1.95 Ga. However, it is important to note that the order of precipitation is dependent on calcium, sodium, and chlorine concentrations, in addition to alkalinity, which are poorly constrained during the Proterozoic (Blättler et al., 2018).

In contrast with this estimate, Shen et al. (2002) proposed a range of 0.5 to 2.4 mM for marine sulphate during the late Paleoproterozoic, based on iron-sulphur chemistry from the McArthur Basin, Australia. Further, the ca. 1.9 Ga Stark Formation, Athapuscow Basin (N.W.T, Canada) originally contained up to several hundred meters of halite (prior to dissolution) with only sparse gypsum pseudomorphs, indicating that halite precipitated prior to gypsum in seawater at this time (Pope and Grotzinger, 2003). Ultimately, this range of estimates highlights the need for holistic, detailed field, geochemical, and geochronological to better resolve ancient marine sulphate concentrations.

5.5. Early Cyanobacteria

Deciphering the ancient cyanobacterial microfossil record has remained a challenge due to their morphological simplicity. While older, more ambiguous fossils exist that may be Cyanobacteria, the Belcher Group preserves the oldest widely accepted cyanobacterial microfossils (Fischer et al., 2016). The cyanobacterial affinity of the microfossil *Eoentophysalis belcherensis* has been inferred from its morphological similarities with modern *Entophysalis* and a similar (paleo)environmental occurrence; both are found in intertidal to shallow subtidal environments, where they form microbial mats and small, laterally linked, domal stromatolites (Hofmann, 1976). Further, *E. belcherensis* has been observed to form colonies of pustulose laminae (Hofmann, 1976), with outward-facing, light-exposed surfaces exhibiting increased staining, interpreted by Golubic and Hofmann (1976) as the UV-blocking pigment scytonemin (Fig. 7). From the detailed description of the type locality presented by Hofmann (1976), the first appearance datum of these microfossils is 588.5 m above the base of section MB1701 (refer to Supplementary Materials for detailed stratigraphic section). From stratigraphic and chemostratigraphic correlation (refer to Supplementary Materials), the type locality is approximately 240 m below the tuff dated as 2015.4 ± 1.8 Ma, and 475 m above the tuff dated as 2018.5 ± 1.0 Ma. These are the first robust age constraints for the earliest microfossil appearance of *E. belcherensis*; assuming constant depositional rate between these two tuffs, *E. belcherensis* first appeared in the fossil record ca. 2016.5 Ma. However, we note that these microfossils occur in black cherts that are very rare in the Kasegalik Formation, suggesting a strong preservation bias.

Based on relaxed molecular clock analyses, it has been argued that crown group Oxyphotobacteria (the clade of Cyanobacteria capable of oxygenic photosynthesis) evolved after the GOE rather than before (Shih et al., 2017). While we cannot distinguish between a crown- versus stem-group Oxyphotobacteria placement for *E. belcherensis*, an age of 2016.5 Ma for the first appearance of total group Oxyphotobacteria fossils is consistent with these molecular clock results (Shih et al., 2017). In any case, these new depositional ages provide a robust minimum age for the earliest appearance of unambiguous cyanobacterial fossils.

6. Conclusions

The new $\delta^{13}C$ and geochronology data presented here support a dynamic Orosirian Earth system, with $\delta^{13}C$ up to +3.6‰. These values are markedly lower than those observed during the preceding LJE, and differ from the subsequent 1.8–1.3 Ga interval in which little systematic variation has been observed. One possible hypothesis for the systematic variation in Orosirian $\delta^{13}C$ is widespread orogenesis leading up to the amalgamation of the Nuna supercontinent, which may have increased nutrient supply and sedimentation rates, that resulted in a relative increase in organic carbon burial. This interpretation places a strong tectonic control on the Orosirian carbon cycle. New depositional ages from two tuffs in the Kasegalik Formation constrain the first appearance of the cyanobacterial microfossil *Eoentophysalis belcherensis* to between 2018.5 ± 1.0 and 2015.4 ± 1.8 Ma, and a tuff at the Flaherty–Omarolluk contact dates orogenesis associated with collision of the Superior and Hearne cratons to have been ongoing ca. 1854.2 ± 1.6 Ma. The 250 Myr interval comprising the Orosirian Period may represent a unique state in the Earth system, between the two extremes of the GOE and LJE, and the hypothesised environmental stability of the late Paleoproterozoic to mid-Mesoproterozoic. Ultimately, further detailed study will help to better understand this 250 Myr interval of Earth history and the transition it records.

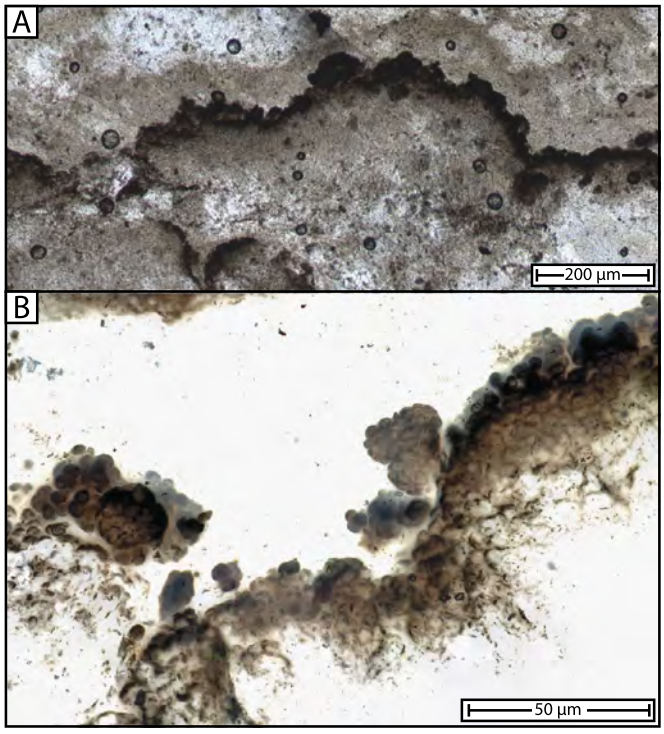

Fig. 7. A) Photomicrograph showing pustulose mats of *Eoentophysalis belcherensis*. These mats exhibit increased pigmentation on their upper surfaces, interpreted by Golubic and Hofmann (1976) as scytonemin. Sample GSC 43590, Geological Survey of Canada. B) Z-stack photomicrograph of *Eoentophysalis belcherensis*, clearly showing individual cells of *Eoentophysalis belcherensis*. Increased pigmentation on the upper surfaces is visible. Sample GSC 43589, Geological Survey of Canada.

Acknowledgements

We thank Thi Hao Bui, Julie Halotel, and Jim Crowley for lab assistance, and Jack Iqaluk, Gary and Alan Rumbolt, Lucassie Ippak, Johnassie Inuktaluk, and Tony Appaqaq for assistance in the field. P.F. Hoffman and P.W. Crockford provided helpful discussion, and input from L.C. Kah and D.A.D. Evans improved an earlier version of the manuscript. Andrey Bekker, Wouter Bleeker, and an anonymous reviewer are thanked for their constructive reviews of this manuscript. Michelle Coyne and the Geological Survey of Canada are thanked for providing thin sections of *Eoentophysalis belcherensis*. MSWH was supported by an NSERC PGS-D, and student re-

search grants from National Geographic, the American Philosophical Society Lewis and Clark Fund, Northern Scientific Training Program, McGill University GREAT, Geological Society of America, Mineralogical Association of Canada, and Stanford University McGee and Compton grants. EAS is supported by the Alfred P. Sloan Foundation. Code used for the LOWESS curve in Fig. 2 was modified from Felix Schönbrodt.

Appendix A. Supplementary material

Supplementary material related to this article can be found online at https://doi.org/10.1016/j.epsl.2019.05.023.

References

Arndt, N., Todt, W., 1994. Formation of 1.9-Ga-old Trans-Hudson continental crust: Pb isotopic data. Chem. Geol. 118, 9–26.
Baragar, W., Scoates, R., 1981. The Circum-Superior belt: a proterozoic plate margin? In: Developments in Precambrian Geology, vol. 4. Elsevier, pp. 297–330.
Barham, M., Kirkland, C., Hollis, J., 2019. Spot the difference: zircon disparity tracks crustal evolution. Geology.
Bekker, A., Holland, H., 2012. Oxygen overshoot and recovery during the early Paleoproterozoic. Earth Planet. Sci. Lett. 317, 295–304.
Bekker, A., Krapež, B., Müller, S.G., Karhu, J.A., 2016. A short-term, post-Lomagundi positive C isotope excursion at c. 2.03 Ga recorded by the Wooly Dolomite, Western Australia. J. Geol. Soc. 173, 689–700.
Bekker, A., Rainbird, R.H., Karhu, J.A., 2007. Linking the Mistassini and Otish basins with the Paleoproterozoic evolution of the Superior Craton. Geological Association of Canada Mineralogical Association of Canada.
Bell, R., Jackson, G., 1974. Aphebian halite and sulphate indications in the Belcher Group, Northwest Territories. Can. J. Earth Sci. 11, 722–728.
Berman, R., Davis, W., Pehrsson, S., 2007. Collisional Snowbird tectonic zone resurrected: growth of Laurentia during the 1.9 Ga accretionary phase of the Hudsonian orogeny. Geology 35, 911–914.
Blättler, C., Claire, M., Prave, A.R., Kirsimäe, K., Higgins, J., Medvedev, P., Romashkin, A., Rychanchik, D., Zerkle, A., Paiste, K., et al., 2018. Two-billion-year-old evaporites capture Earth's great oxidation. Science 360, 320–323.
Brand, U., Veizer, J., 1980. Chemical diagenesis of a multicomponent carbonate system, 1: trace elements. J. Sediment. Res. 50, 1219–1236.
Brasier, M., Lindsay, J., 1998. A billion years of environmental stability and the emergence of eukaryotes: new data from northern Australia. Geology 26, 555–558.
Buchan, K.L., Mortensen, J.K., Card, K.D., Percival, J.A., 1998. Paleomagnetism and U–Pb geochronology of diabase dyke swarms of Minto block, Superior Province, Quebec, Canada. Can. J. Earth Sci. 35, 1054–1069.
Canfield, D.E., 1994. Factors influencing organic carbon preservation in marine sediments. Chem. Geol. 114, 315–329.
Canfield, D.E., 2005. The early history of atmospheric oxygen: homage to Robert M. Garrels. Annu. Rev. Earth Planet. Sci. 33, 1–36.
Chandler, F., Parrish, R., 1989. Age of the Richmond Gulf Group and implications for rifting in the Trans-Hudson Orogen, Canada. Precambrian Res. 44, 277–288.
Condon, D., Schoene, B., McLean, N., Bowring, S., Parrish, R., 2015. Metrology and traceability of U–Pb isotope dilution geochronology (EARTHTIME Tracer Calibration Part I). Geochim. Cosmochim. Acta 164, 464–480.
Crockford, P.W., Hayles, J.A., Bao, H., Planavsky, N.J., Bekker, A., Fralick, P.W., Halverson, G.P., Bui, T.H., Peng, Y., Wing, B.A., 2018. Triple oxygen isotope evidence for limited mid-Proterozoic primary productivity. Nature 559, 613.
Ernst, R., Bleeker, W., 2010. Large igneous provinces (LIPs), giant dyke swarms, and mantle plumes: significance for breakup events within Canada and adjacent regions from 2.5 Ga to the Present. Can. J. Earth Sci. 47, 695–739.
Fiorella, R.P., Sheldon, N.D., 2017. Equable end Mesoproterozoic climate in the absence of high CO_2. Geology 45, 231–234.
Fischer, W.W., Hemp, J., Johnson, J.E., 2016. Evolution of oxygenic photosynthesis. Annu. Rev. Earth Planet. Sci. 44, 647–683.
France-Lanord, C., Derry, L.A., 1997. Organic carbon burial forcing of the carbon cycle from Himalayan erosion. Nature 390, 65.
Gibson, T.M., Shih, P.M., Cumming, V.M., Fischer, W.W., Crockford, P.W., Hodgskiss, M.S., Wörndle, S., Creaser, R.A., Rainbird, R.H., Skulski, T.M., et al., 2017. Precise age of Bangiomorpha pubescens dates the origin of eukaryotic photosynthesis. Geology 46, 135–138.
Golubic, S., Hofmann, H., 1976. Comparison of Holocene and mid-Precambrian Entophysalidaceae (Cyanophyta) in stromatolitic algal mats: cell division and degradation. J. Paleontol., 1074–1082.
Gumsley, A.P., Chamberlain, K.R., Bleeker, W., Söderlund, U., de Kock, M.O., Larsson, E.R., Bekker, A., 2017. Timing and tempo of the Great Oxidation Event. Proc. Natl. Acad. Sci. USA 114, 1811–1816.
Guo, H., Du, Y., Kah, L.C., Huang, J., Hu, C., Huang, H., Yu, W., 2013. Isotopic composition of organic and inorganic carbon from the Mesoproterozoic Jixian Group, North China: implications for biological and oceanic evolution. Precambrian Res. 224, 169–183.
Hamilton, M., Buchan, K., Ernst, R., Stott, G., 2009. Widespread and short-lived 1870 Ma mafic magmatism along the northern Superior craton margin. In: American Geophysical Union-Geological Association of Canada Joint Meeting (abstract# GA11A-01).
Hamilton, M.A., Goutier, J., Buchan, K.L., 2016. Minto Large Igneous Province: a 2.00 Ga Mafic Magmatic Event in the eastern Superior Craton based on U–Pb baddeleyite geochronology and paleomagnetism. Acta Geol. Sin., English Ed. 1, 69–70.
Hedges, J.I., Keil, R.G., 1995. Sedimentary organic matter preservation: an assessment and speculative synthesis. Mar. Chem. 49, 81–115.
Heimann, A., Johnson, C.M., Beard, B.L., Valley, J.W., Roden, E.E., Spicuzza, M.J., Beukes, N.J., 2010. Fe, C, and O isotope compositions of banded iron formation carbonates demonstrate a major role for dissimilatory iron reduction in ~2.5 Ga marine environments. Earth Planet. Sci. Lett. 294, 8–18.
Hiess, J., Condon, D.J., McLean, N., Noble, S.R., 2012. $^{238}U/^{235}U$ systematics in terrestrial uranium-bearing minerals. Science 335, 1610–1614.
Hoffman, P.F., 1987. Early Proterozoic foredeeps, foredeep magmatism, and Superior-type iron-formations of the Canadian Shield. In: Proterozic Lithospheric Evolution, vol. 17, pp. 85–98.
Hoffman, P.F., Bowring, S.A., Buchwaldt, R., Hildebrand, R.S., 2011. Birthdate for the Coronation paleocean: age of initial rifting in Wopmay orogen, Canada. Can. J. Earth Sci. 48, 281–293.
Hofmann, H., 1976. Precambrian microflora, Belcher Islands, Canada: significance and systematics. J. Paleontol., 1040–1073.
Hotinski, R., Kump, L., Arthur, M., 2004. The effectiveness of the Paleoproterozoic biological pump: a $\delta^{13}C$ gradient from platform carbonates of the Pethei Group (Great Slave Lake Supergroup, NWT). Geol. Soc. Am. Bull. 116, 539–554.
Jackson, G.D., 1960. Belcher Islands, Northwest Territories, 33 M, 34 D, E. Technical Report. Geological Survey of Canada.
Jackson, G.D., 2013. Geology, Belcher Islands, Nunavut. Technical Report Open-File Report 4923. Geological Survey of Canada.
Kah, L.C., Lyons, T.W., Chesley, J.T., 2001. Geochemistry of a 1.2 Ga carbonate-evaporite succession, northern Baffin and Bylot Islands: implications for Mesoproterozoic marine evolution. Precambrian Res. 111, 203–234.
Karhu, J.A., Holland, H.D., 1996. Carbon isotopes and the rise of atmospheric oxygen. Geology 24, 867–870.
Kolb, J., 2014. Structure of the Palaeoproterozoic Nagssugtoqidian Orogen, South-East Greenland: model for the tectonic evolution. Precambrian Res. 255, 809–822.
Krogh, T., Davis, D., Corfu, F., et al., 1984. Precise U–Pb Zircon and Baddeleyite Ages for the Sudbury Area. Technical Report. Ontario Geological Survey.
Kunzmann, M., Schmid, S., Blaikie, T.N., Halverson, G.P., 2019. Facies analysis, sequence stratigraphy, and carbon isotope chemostratigraphy of a classic Zn-Pb host succession: the Proterozoic middle McArthur Group, McArthur Basin, Australia. Ore Geol. Rev.
Land, L.S., 1980. The isotopic and trace element geochemistry of dolomite: the state of the art. Spec. Publ., Soc. Econ. Paleontol. Mineral. 28, 87–110.
Lindsay, J.F., Brasier, M.D., 2002. Did global tectonics drive early biosphere evolution? Carbon isotope record from 2.6 to 1.9 Ga carbonates of Western Australian basins. Precambrian Res. 114, 1–34.
Macdonald, F.A., Schmitz, M.D., Strauss, J.V., Halverson, G.P., Gibson, T.M., Eyster, A., Cox, G., Mamrol, P., Crowley, J.L., 2018. Cryogenian of Yukon. Precambrian Res. 319, 114–143.
Mattinson, J.M., 2010. Analysis of the relative decay constants of ^{235}U and ^{238}U by multi-step CA-TIMS measurements of closed-system natural zircon samples. Chem. Geol. 275, 186–198.
McLean, N.M., Condon, D.J., Schoene, B., Bowring, S.A., 2015. Evaluating uncertainties in the calibration of isotopic reference materials and multi-element isotopic tracers (EARTHTIME Tracer Calibration Part II). Geochim. Cosmochim. Acta 164, 481–501.
Miyazaki, Y., Planavsky, N.J., Bolton, E.W., Reinhard, C.T., 2018. Making sense of massive carbon isotope excursions with an inverse carbon cycle model. J. Geophys. Res., Biogeosci. 123, 2485–2496.
Moecher, D.P., Samson, S.D., 2006. Differential zircon fertility of source terranes and natural bias in the detrital zircon record: implications for sedimentary provenance analysis. Earth Planet. Sci. Lett. 247, 252–266.
Pehrsson, S.J., Eglington, B.M., Evans, D.A., Huston, D., Reddy, S.M., 2016. Metallogeny and its link to orogenic style during the Nuna supercontinent cycle. Geol. Soc. (Lond.) Spec. Publ. 424, 83–94.
Pope, M.C., Grotzinger, J.P., 2003. Paleoproterozoic Stark Formation, Athapuscow basin, northwest Canada: record of cratonic-scale salinity crisis. J. Sediment. Res. 73, 280–295.
Rasmussen, B., Fletcher, I.R., Bekker, A., Muhling, J.R., Gregory, C.J., Thorne, A.M., 2012. Deposition of 1.88-billion-year-old iron formations as a consequence of rapid crustal growth. Nature 484, 498.
Ricketts, B., 1979. Sedimentology and Stratigraphy of Eastern and Central Belcher Islands, Northwest Territories. Ph.D. Thesis. Carleton University.
Schmidt, P., 1980. Paleomagnetism of igneous rocks from the Belcher Islands, Northwest Territories, Canada. Can. J. Earth Sci. 17, 807–822.

Schoene, B., Crowley, J.L., Condon, D.J., Schmitz, M.D., Bowring, S.A., 2006. Reassessing the uranium decay constants for geochronology using ID-TIMS U–Pb data. Geochim. Cosmochim. Acta 70, 426–445.

Schröder, S., Bekker, A., Beukes, N., Strauss, H., Van Niekerk, H., 2008. Rise in seawater sulphate concentration associated with the Paleoproterozoic positive carbon isotope excursion: evidence from sulphate evaporites in the 2.2–2.1 Gyr shallow-marine Lucknow Formation, South Africa. Terra Nova 20, 108–117.

Scott, C., Wing, B.A., Bekker, A., Planavsky, N.J., Medvedev, P., Bates, S.M., Yun, M., Lyons, T.W., 2014. Pyrite multiple-sulfur isotope evidence for rapid expansion and contraction of the early Paleoproterozoic seawater sulfate reservoir. Earth Planet. Sci. Lett. 389, 95–104.

Shen, Y., Canfield, D.E., Knoll, A.H., 2002. Middle Proterozoic ocean chemistry: evidence from the McArthur Basin, northern Australia. Am. J. Sci. 302, 81–109.

Shields, G., Veizer, J., 2002. Precambrian marine carbonate isotope database: version 1.1. Geochem. Geophys. Geosyst. 3, 1–12.

Shih, P., Hemp, J., Ward, L., Matzke, N., Fischer, W., 2017. Crown group Oxyphotobacteria postdate the rise of oxygen. Geobiology 15, 19–29.

Skipton, D., Schneider, D., McFarlane, C., St-Onge, M., Jackson, S., 2016. Multi-stage zircon and monazite growth revealed by depth profiling and in situ U–Pb geochronology: resolving the Paleoproterozoic tectonics of the Trans-Hudson Orogen on southeastern Baffin Island, Canada. Precambrian Res. 285, 272–298.

Steiger, R., Jäger, E., 1977. Subcommission on geochronology: convention on the use of decay constants in geo- and cosmochronology. Earth Planet. Sci. Lett. 36, 359–362.

Tirrul, R., Grotzinger, J.P., 1990. Early Proterozoic collisional orogeny along the northern Thelon tectonic zone, Northwest Territories, Canada: evidence from the foreland. Tectonics 9, 1015–1036.

Turner, E., Bekker, A., 2016. Thick sulfate evaporite accumulations marking a mid-Neoproterozoic oxygenation event (Ten Stone Formation, Northwest Territories, Canada). Geol. Soc. Am. Bull. 128, 203–222.

Voice, P.J., Kowalewski, M., Eriksson, K.A., 2011. Quantifying the timing and rate of crustal evolution: global compilation of radiometrically dated detrital zircon grains. J. Geol. 119, 109–126.

Waldbauer, J.R., Chamberlain, C.P., 2005. Influence of uplift, weathering, and base cation supply on past and future CO_2 levels. In: A History of Atmospheric CO_2 and Its Effects on Plants, Animals, and Ecosystems. Springer, pp. 166–184.

Wardle, R.J., James, D.T., Scott, D.J., Hall, J., 2002. The southeastern Churchill Province: synthesis of a Paleoproterozoic transpressional orogen. Can. J. Earth Sci. 39, 639–663.

Weller, O., St-Onge, M., 2017. Record of modern-style plate tectonics in the Palaeoproterozoic Trans-Hudson orogen. Nat. Geosci. 10, 305.

Whitmeyer, S.J., Karlstrom, K.E., 2007. Tectonic model for the Proterozoic growth of North America. Geosphere 3, 220–259.

Wilson, J.P., Fischer, W.W., Johnston, D.T., Knoll, A.H., Grotzinger, J.P., Walter, M.R., McNaughton, N.J., Simon, M., Abelson, J., Schrag, D.P., et al., 2010. Geobiology of the late Paleoproterozoic Duck Creek Formation, Western Australia. Precambrian Res. 179, 135–149.